PHYSICAL REVIEW B **95**, 140405(R) (2017)

Domain-wall dynamics in magnetoelastic nanostripes

Théo Mathurin, Stefano Giordano,* Yannick Dusch, Nicolas Tiercelin, Philippe Pernod, and Vladimir Preobrazhensky
Institute of Electronics, Microelectronics and Nanotechnology - UMR 8520, LIA LICS, Université Lille, CNRS, Centrale Lille, ISEN, Université Valenciennes, F-59000 Lille, France

(Received 14 November 2016; published 25 April 2017)

We numerically demonstrate the possibility to manipulate domain walls in magnetoelastic nanostripes by means of uniform mechanical stresses. The symmetry breaking of the magnetic states in unidimensional ferromagnets allows the control of the domain-wall position or velocity in geometrically tailored nanostripes coupled to piezoelectric substrates. We further predict that this approach yields unusual domain-wall configurations with velocities of the same order of magnitude as that induced by magnetic fields or spin-polarized currents, while the energy consumption is considerably smaller.

DOI: 10.1103/PhysRevB.95.140405

Magnetic domain walls (DWs), localized structures separating regions of different magnetization in ferromagnets, can be controlled and moved in nanowires or nanostripes, e.g., to store [1–4] or process [5–8] information. For this purpose, DW motion can be typically induced by external magnetic fields [9–12] or spin-polarized currents [13–18]. However, in order to reduce energy consumption in these systems, there is considerable interest in the use of mechanical actions (generated by electric fields), instead of electric currents. This is a very challenging task since a uniform stress does not directly induce unidirectional motion of head-to-head (180°) DWs. For this reason, the mechanical coupling has been proposed in complex heterostructures of rather convoluted realization and operation. For instance, a localized nonuniform mechanical stress has been exploited to move a DW in a nanowire sandwiched between a substrate and a multicontacted piezoelectric layer [19,20]. A recent application of this principle has been exploited to produce the rotation of a DW in a ferromagnetic ring fabricated on a piezoelectric substrate [21,22]. Also, the mobility of a current- or field-induced DW can be piezoelectrically controlled through a strain-mediated magnetic anisotropy [23–26]. Moreover, magnetic DW motion can be caused by pinning onto moving ferroelectric DWs [27,28]. The strain-mediated electric control of domain structures can also be achieved for domain walls between orthogonal states (90°) in cubic ferromagnets in the absence of external magnetic field [29]. A promising alternative is based on the symmetry breaking of the two opposite stable magnetization states arising from the uniaxial anisotropy of unidimensional ferromagnets. Basically, this can be realized through a static magnetic field, e.g., generated by permanent magnets, which is perpendicularly applied to the ferromagnetic easy axis. The consequent tilting of the states allows for their manipulation by way of uniform mechanical actions. This mechanism has been used to mechanically switch the magnetization of magnetoelastic particles [30–37] or to induce DW displacement with uniform stresses [38,39].

In this Rapid Communication we investigate the distinctive DW dynamics induced in an amorphous magnetoelastic nanostripe by this mechanism, i.e., by the combination of a bias magnetic field $\vec{H}_0$ and a uniform stress generated by a piezoelectric substrate [see Fig. 1(a)]. The applied stress considered is composed of uniform orthogonal tensile and compressive components [σ and τ in Fig. 1(b)], and is controlled by an electric field $\vec{E}_0$ via the piezoelectric effect. We provide evidence that the DW velocity is of the same order of magnitude as that of field- or current-induced motion, while the energy consumption is between one and two orders of magnitude smaller. Tailoring of the static and dynamic responses is possible through the engineering of the cross section. We will discuss the parabolic and constant-section profiles, leading to a precise position and velocity control, respectively. In particular, the parabolic profile yields a reversible behavior with a one-to-one correspondence between applied stress (or electric field) and DW position [see Fig. 1(c)]. It is worth noticing that contrary to the well-known steady-state Walker DW dynamics, where the magnetization is always contained in a given plane [40], we observe here local out-of-plane excursions of the magnetization vector during its evolution.

To model the system dynamics, we assume that the magnetization $\vec{M}$ depends only on x and t. Therefore, we can write $\vec{M} = M_s\vec{\gamma}$, where M_s is the magnetization at saturation and $\vec{\gamma} = (\cos\Phi\sin\Theta, \sin\Phi\sin\Theta, \cos\Theta)$ is a unit vector with $\Phi = \Phi(x,t)$ and $\Theta = \Theta(x,t)$ [see Fig. 1(a)]. The total energy density $u = u_{\rm an} + u_{\rm Ze} + u_{\rm de} + u_{\rm ex} + u_{\rm me}$ within the nanostripe is composed of the following terms. The uniaxial anisotropy along x is given by $u_{\rm an} = -K_u\gamma_x^2$, while the Zeeman contribution corresponds to $u_{\rm Ze} = -\mu_0 M_S H_0\gamma_y$. Similarly, the demagnetization energy density is $u_{\rm de} = -\frac{1}{2}\mu_0 M_s\vec{H}_d\cdot\vec{\gamma}$, where $\vec{H}_d$ is the demagnetization field $\vec{H}_d(\vec{r}) = M_S\int_\Omega \overleftrightarrow{N}(\vec{r},\vec{r}_0)\vec{\gamma}(\vec{r}_0)d\vec{r}_0$ (here $\overleftrightarrow{N}$ is the demagnetization tensor [38,39], and Ω is the whole magnetoelastic region). The exchange energy density can be written as $u_{\rm ex} = A(d\vec{\gamma}/dx)^2$, where A is the exchange coefficient. The general form of the magnetoelastic energy density is $u_{\rm me} = -T_{ij}\epsilon_{ij}^{\mu}$, where T_{ij} is the local Cauchy stress tensor and $\epsilon_{ij}^{\mu}(\vec{\gamma})$ is the magnetostrictive strain. Its mathematical expression is $\epsilon_{ij}^{\mu} = \frac{\lambda_S}{2}(3\gamma_i\gamma_j - \delta_{ij})$, where λ_S is the magnetostriction coefficient. The elastic and magnetoelastic properties of the ferromagnetic stripe are assumed to be isotropic (amorphous ferromagnets). With the geometry of Fig. 1, we obtain $u_{\rm me} = -\frac{3}{4}\lambda_S[(\tau+\sigma)(\gamma_x^2+\gamma_y^2) + 2(\tau-\sigma)\gamma_x\gamma_y]$, where τ and σ are

*Stefano.Giordano@iemn.univ-lille1.fr

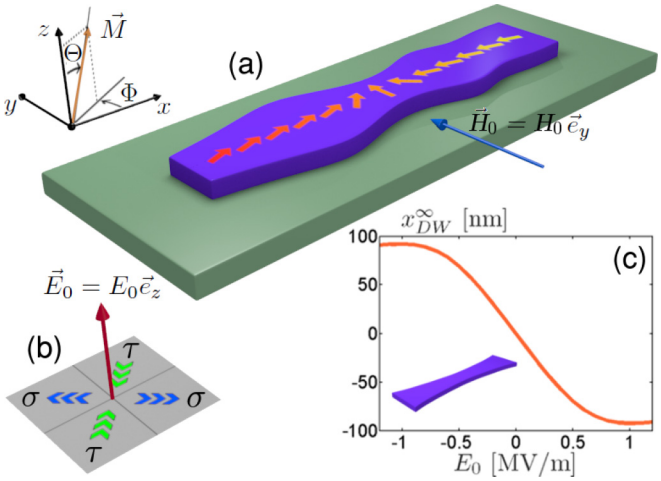

FIG. 1. (a) Sketch of the system constituted by a magnetoelastic nanostripe deposited on a piezoelectric substrate. The magnetization vector $\vec{M}$ is described by angles Φ and Θ and the nanostripe easy axis is along x. A DW is thus created between two states tilted by the magnetic field $\vec{H}_0$. (b) Stress components $\sigma > 0$ and $\tau < 0$ generated by the electric field $\vec{E}_0 = E_0\vec{e}_z$ with $E_0 > 0$ (if $E_0 < 0$, then $\sigma < 0$ and $\tau > 0$). (c) DW equilibrium position versus electric field in a nanostripe with parabolic shape.

the stress components along $\vec{e}_\tau = (\vec{e}_x + \vec{e}_y)/\sqrt{2}$ and $\vec{e}_\sigma = (\vec{e}_y - \vec{e}_x)/\sqrt{2}$, respectively ($\vec{e}_i$ is the unit vector along the i axis). Their values are defined by $\tau = 2\mu E_0(d_{31} + \nu d_{32})/(1-\nu)$ and $\sigma = 2\mu E_0(d_{32} + \nu d_{31})/(1-\nu)$. Here μ and ν are the shear modulus and the Poisson ratio of the magnetoelastic nanostripe and d_{31} and d_{32} are the piezoelectric coefficients of the substrate. They control the strains $\varepsilon_\tau = d_{31}E_0$ and $\varepsilon_\sigma = d_{32}E_0$, along $\vec{e}_\tau$ and $\vec{e}_\sigma$, respectively, transmitted without loss to the nanostripe. Although the spatial uniformity of stresses τ and σ and of the magnetic field $\vec{H}_0$ may not be rigorously fulfilled in real structures because of experimental constraints, we choose to consider uniform fields in order to shed light on the peculiar physics generated by the coexistence of τ, σ, and $\vec{H}_0$ [41]. Presumably, the resulting behavior would be only slightly altered as the model is made more realistic. For the same reason, the edge roughness, possibly generating potential wells for the DW [42], is also here neglected.

The application of the variational calculus to the total energy $U = \int_\Omega u dv$, Ω being the region defined by $-\frac{L}{2} \leqslant x \leqslant +\frac{L}{2}$, $-\frac{\ell(x)}{2} \leqslant y \leqslant +\frac{\ell(x)}{2}$, and $-\frac{h}{2} \leqslant z \leqslant +\frac{h}{2}$, yields the static or equilibrium equation $\vec{\gamma} \wedge \vec{H}_{\rm eff} = 0$, where the effective field $\vec{H}_{\rm eff}$ is given by

$$\vec{H}_{\rm eff} = H_0\vec{e}_y + \langle\vec{H}_d\rangle + \frac{2K_u\gamma_x\vec{e}_x}{\mu_0 M_S} + \frac{2A}{\mu_0 M_S \ell}\frac{\partial}{\partial x}\left(\ell\frac{\partial\vec{\gamma}}{\partial x}\right) + \frac{3\sqrt{2}\lambda_S}{2\mu_0 M_S}[(\gamma_x+\gamma_y)\tau\vec{e}_\tau - (\gamma_x-\gamma_y)\sigma\vec{e}_\sigma], \quad (1)$$

and $\ell(x)$ is the profile of the variable section. Here $\langle\vec{H}_d\rangle$ represents the average value of $\vec{H}_d$ on the (y,z) cross section of the nanostripe. The effective field $\vec{H}_{\rm eff}$ can now be inserted into the Landau-Lifshitz-Gilbert (LLG) equation, describing the magnetization dynamics [43,44]. We eventually obtain its explicit form

$$\dot{\Phi} = \mathsf{G}(\alpha\mathsf{r} - \mathsf{s})/\sin\Theta, \qquad \dot{\Theta} = \mathsf{G}(\alpha\mathsf{s} + \mathsf{r}), \quad (2)$$

where α is the damping coefficient, $\mathsf{G} = \mu_0\mathcal{G}/(1+\alpha^2)$, $\mathcal{G} = 1.76 \times 10^{11}$ rad s^{-1} T^{-1} is the electron gyromagnetic ratio, and r and s follow

$$\begin{aligned}\mathsf{r} = &-\sin\Phi\langle H_{dx}\rangle + \cos\Phi\langle H_{dy}\rangle + \cos\Phi H_0 \\ &- \frac{2K_u}{\mu_0 M_S}\cos\Phi\sin\Phi\sin\Theta \\ &+ \frac{3}{2}\frac{\lambda_S}{\mu_0 M_S}(\tau-\sigma)\cos(2\Phi)\sin\Theta \\ &+ \frac{2A}{\mu_0 M_S}\left(\frac{\ell'}{\ell}\Phi'\sin\Theta + 2\Phi'\Theta'\cos\Theta + \Phi''\sin\Theta\right), \quad (3)\end{aligned}$$

$$\begin{aligned}\mathsf{s} = &\cos\Phi\cos\Theta\langle H_{dx}\rangle + \sin\Phi\cos\Theta\langle H_{dy}\rangle - \sin\Theta\langle H_{dz}\rangle \\ &+ \sin\Phi\cos\Theta H_0 + \frac{2K_u}{\mu_0 M_S}\cos^2\Phi\sin\Theta\cos\Theta \\ &+ \frac{3}{2}\frac{\lambda_S}{\mu_0 M_S}\cos\Theta\sin\Theta[(\tau+\sigma) + \sin(2\Phi)(\tau-\sigma)] \\ &+ \frac{2A}{\mu_0 M_S}\left(\frac{\ell'}{\ell}\Theta' + \Theta'' - \Phi'^2\cos\Theta\sin\Theta\right). \quad (4)\end{aligned}$$

Here $\dot{f} \equiv \partial f/\partial t$ and $f' \equiv \partial f/\partial x$. Since $\langle\vec{H}_d\rangle$ is given by an integral expression depending on Θ and Φ, Eqs. (2)–(4) represent a system of two strongly nonlinear partial integrodifferential equations. To solve it, we developed an *ad hoc* numerical procedure based on an implicit nonlinear finite difference scheme combined with a precise calculation of the actual demagnetization field [39]. This methodology has been successfully tested against the exact Walker solution, describing the dynamics of a DW driven by a magnetic field [40]. Moreover, solutions have been validated by testing their stability to large variations of the time step Δt and the discretization interval Δx, and by the comparison with micromagnetic simulations [41].

A $TbCo_2$/FeCo multilayered nanostripe with $M_s = 64 \times 10^4$ A/m, $A = 9 \times 10^{-12}$ J/m, $\mu = 80$ GPa, $\nu = 0.25$, $\lambda_S = 2 \times 10^{-4}$ [38] is the representative nanomagnet. We use $K_u = 37.5 \times 10^3$ J/m^3, $H_0 = 20 \times 10^3$ A/m, and $0.06 \leqslant \alpha \leqslant 0.12$, which are reasonable values in real systems. We also adopt the piezoelectric PMN-PT ceramic with $d_{32} = 600$ pC/N and $d_{31} = -1900$ pC/N [45].

We first discuss a parabola shaped nanostripe with thickness $h = 10$ nm and $\ell(x) = a + 4\frac{b-a}{L^2}x^2$, where $a = \ell(0) = 40$ nm (central width), $b = \ell(\pm L/2) = 70$ nm (width at extremities), and $L = 400$ nm [see Fig. 2(a)]. If $\vec{H}_0 = 0$ and $\vec{E}_0 = 0$, we consider a Néel DW at $x = 0$, between two domains of opposite magnetization (initial metastable condition). If $\vec{H}_0 \neq 0$ the states are tilted but still have the same energy, keeping the DW at $x = 0$. This equilibrium configuration is found with a nonlinear relaxation method applied to the equations $\mathsf{r} = 0$ and $\mathsf{s} = 0$ [38,39], and is taken as initial condition to analyze the dynamics through Eq. (2). Indeed, when $\vec{E}_0 \neq 0$ is applied, the DW moves so as to reduce the

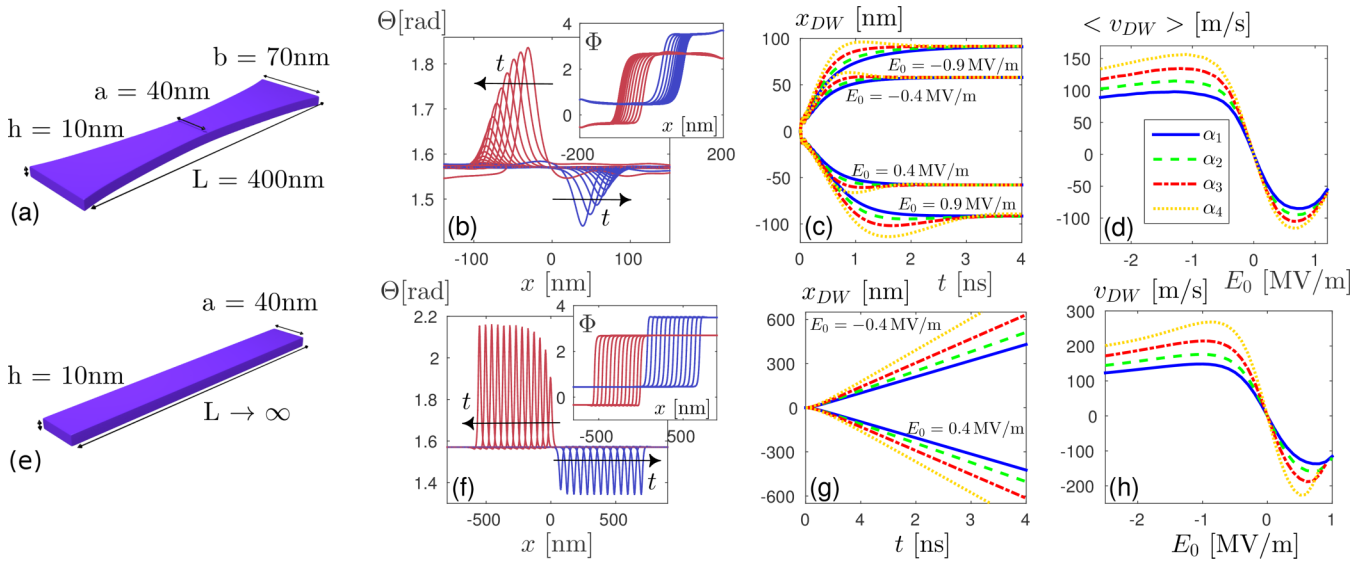

FIG. 2. Dynamics of the magnetic DW in the nanostripe with parabolic (a) and constant (e) section. (b) and (f) Evolution of the magnetization angles $\Theta(x,t)$ and $\Phi(x,t)$ (inset) obtained with $E_0 = \pm 0.8$ MV/m and the damping parameter $\alpha = 0.1$ (angles versus x at different times t). If $E_0 > 0$, the DW moves to the left ($x < 0$), and if $E_0 < 0$, the DW moves to the right ($x > 0$). (c) and (g) Time evolution of x_{DW} for $\alpha_1 = 0.12$, $\alpha_2 = 0.1$, $\alpha_3 = 0.08$, and $\alpha_4 = 0.06$ and for the indicated values of E_0. (d) and (h) Asymmetric behavior of the DW velocity (average value $\langle v_{\mathrm{DW}} \rangle$ for the parabolic nanostripe and steady-state value v_{DW} for the uniform nanostripe) versus electric field E_0 for the above values of α.

size of the domain with higher energy density. By virtue of the adopted geometry with variable section, the DW reaches a final equilibrium position $x_{\mathrm{DW}}^{\infty} = \lim_{t\to\infty} x_{\mathrm{DW}}(t)$ depending on the strength of E_0 [see Fig. 1(c)]. There is in fact an exchange energy cost to increase its surface. The DW position can thus be unequivocally controlled and is symmetric for opposite values of E_0 [see again Fig. 1(c)].

Contrary to the static response, the dynamics described by $\Phi = \Phi(x,t)$ and $\Theta = \Theta(x,t)$ [see Fig. 2(b)] and $x_{\mathrm{DW}}(t)$ [see Fig. 2(c)] exhibits a remarkable asymmetry between $E_0 > 0$ and $E_0 < 0$. This intriguing behavior is caused by the disparity $d_{32} \neq -d_{31}$. Indeed, σ and τ fulfill the relation $|\tau| > |\sigma|$ (and they are always of opposite sign). It means that if $E_0 > 0$, the DW moves to the left ($x < 0$) with a compression $|\tau|$ larger than the tension σ; conversely, if $E_0 < 0$, the DW moves to the right ($x > 0$) with a tension τ larger than the compression $|\sigma|$. Since a compression induces a *planar anisotropy* from the magnetic point of view (perpendicularly to its direction) and a traction induces an *axial anisotropy* for the magnetization (along its direction), the motions to the left and to the right are not dynamically equivalent. They are so only if $d_{32} = -d_{31}$, when the identity $\tau = -\sigma$ is verified. In both directions of motion, unusual out-of-plane excursions appear locally. When the compression is larger than the tension ($E_0 > 0$), the prevailing planar anisotropy induces out-of-plane excursions with considerable deviation of Θ from $\pi/2$ [see Fig. 2(a), $x < 0$], and the DW propagation is sensibly hindered [46]. On the other hand, when the tension is larger than the compression ($E_0 < 0$), the out-of-plane excursions are comparatively reduced [see Fig. 2(a), $x > 0$], and the DW motion is facilitated. As shown in Fig. 2(d), this phenomenon is more intense for large values of $|E_0|$. In Fig. 2(d) the quantity $\langle v_{\mathrm{DW}} \rangle$ is defined as the average velocity over the path from the origin to the position $\frac{2}{3}x_{\mathrm{DW}}^{\infty}$. While for $E_0 < 0$, with increasing $|E_0|$ we observe a maximum of $\langle v_{\mathrm{DW}} \rangle$ and a following slight velocity decrease, for $E_0 > 0$ increasing values of E_0 lead to a minimum of $\langle v_{\mathrm{DW}} \rangle$ immediately followed by a strong velocity reduction. This is consistent with the previous interpretation based on the magnetic planar and axial anisotropy. Noteworthy, for $|E_0| < 0.6$ MV/m, we have a quite linear and symmetric response, a convenient feature for technological applications. This point is substantiated by calculating the energy consumption for moving the DW from $x_{\mathrm{DW}}^{\infty}(-E_0)$ to $x_{\mathrm{DW}}^{\infty}(+E_0)$. The magnetic dissipation for the case with $E_0 = 0.4$ MV/m and $x_{DW}^{\infty} = \pm 60$ nm corresponds to $E_m = 10^{-3}$ fJ. Moreover, if we consider a cubic piezoelectric substrate of side $d = 800$ nm with relative permittivity $\varepsilon_r = 3500$, the electric energy consumed is $E_e = CV^2 = \varepsilon_0 \varepsilon_r d^3 E_0^2$ (where $C = \varepsilon_0 \varepsilon_r d$ and $V = E_0 d$). With $E_0 = 0.4$ MV/m, we obtain $E_e = 2.5$ fJ $\gg E_m$ for a DW displacement of 120 nm for this geometry. If permanent magnets generate $\vec{H}_0$ [47], they do not dissipate energy. To draw a comparison, an energy consumption of 200 fJ has been reported to propagate a DW for a distance of 500 nm through spin-polarized currents [18,22]. Then, in the latter case the dissipation per unit length is about 20 times higher.

From a fundamental perspective, our results for the parabolic profile revealed a specific magnetic configuration with an out-of-plane excursion ($\Theta \neq \pi/2$) in proximity to the DW. In order to further investigate this point, we analyzed the DW propagation in a constant-section infinitely long nanostripe [see Fig. 2(e)], and we confirmed the existence of an unusual out-of-plane excursion [41]. This dynamics is therefore substantially richer than the classical Walker propagation [40]. We observe the existence of a rapidly reached steady-state regime, characterized by $\Phi(x,t) = \Phi_0(x - v_{\mathrm{DW}}t)$ and $\Theta(x,t) = \Theta_0(x - v_{\mathrm{DW}}t)$ [see Fig. 2(f)], where Φ_0 and Θ_0 represent the stationary shapes. The corresponding uniformity

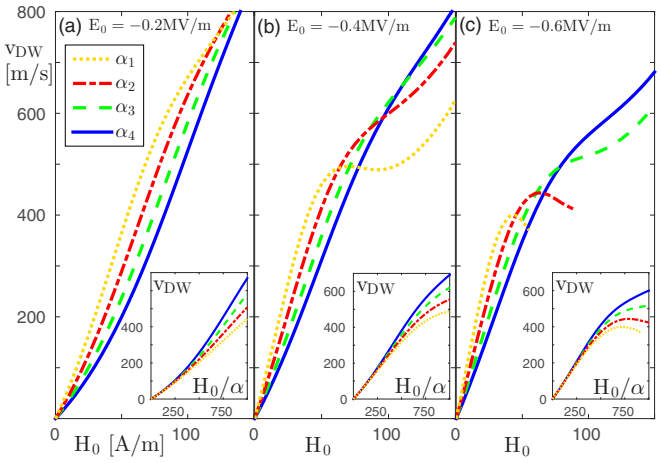

FIG. 3. Velocity of the DW in a constant-section infinitely long nanostripe in terms of H_0 and α for $E_0 = -0.2$ MV/m (a), $E_0 = -0.4$ MV/m (b), and $E_0 = -0.6$ MV/m (c). In the insets the collapse of the linear regime obtained by plotting v_{DW} versus H_0/α is shown. In all panels we used the same values of α introduced in Fig. 2.

of the motion is shown in Fig. 2(g), the steady-state velocity v_{DW} being plotted versus the applied field E_0 in Fig. 2(h). In particular, Fig. 2(h) shows that the constant-section nanostripe exhibits the same asymmetric velocity behavior, already observed and analyzed for the parabolic nanostripe. This configuration allows the control of the DW velocity with the applied electric field.

Further enhancement of magnetic DW dynamics is possible by optimizing the bias magnetic field $\vec{H}_0$. We show in Fig. 3 the DW velocity versus the intensity H_0 in the constant-section nanostripe for the same values of α adopted in Fig. 2 and for three different values of E_0. We deduce that our mechanically induced steady-state regime yields propagation velocities larger than 500 m/s, which are comparable to those obtained by current-driven DW motion [17,18]. In the classical field-induced Walker propagation the dependence of the DW velocity on H_0 and α is mediated by the single variable H_0/α [40]. Hence, we plot v_{DW} versus the ratio H_0/α in the insets of Fig. 3. We observe that the curves corresponding to different α collapse to a single universal response in the linear region. We also note that $\partial v_{DW}/\partial\rho$ (for low values of $\rho = H_0/\alpha$) is an increasing function of E_0, as expected. However, for higher values of the magnetic field, v_{DW} depends on both H_0/α and α, proving once again the essential difference between the mechanically induced and the field-induced DW motion.

In conclusion, we numerically demonstrated that the mechanical manipulation of DWs in magnetoelastic nanostripes can be simply achieved through uniform stresses if we break the symmetry of the states. The resulting moving magnetic structure, characterized by very-low energy dissipation and competitive velocities, is fundamentally different from usual DW in nanostripes, being characterized by specific out-of-plane phenomena. The tailoring of the variable nanostripe section allows one to precisely design static and dynamic features. For instance, the applied electric field may control the DW position in parabolic nanostripes or the DW velocity in uniform nanostripes. Furthermore, complex profiles $\ell(x)$ with two or more minima can be considered to design hysteretic bistable or multistable systems. The DW motion driven by uniform mechanical stress thus deserves experimental investigation for both fundamental physics and applications.

[1] S. S. Parkin, M. Hayashi, and L. Thomas, Science **320**, 190 (2008).
[2] J. H. Franken, H. J. M. Swagten, and B. Koopmans, Nat. Nanotechnol. **7**, 499 (2012).
[3] S. Parkin and S.-H. Yang, Nat. Nanotechnol. **10**, 195 (2015).
[4] Y. P. Ivanov, A. Chuvilin, S. Lopatin, and J. Kosel, ACS Nano **10**, 5326 (2016).
[5] D. A. Allwood, G. Xiong, C. Faulkner, D. Atkinson, D. Petit, and R. P. Cowburn, Science **309**, 1688 (2005).
[6] B. Behin-Aein, D. Datta, S. Salahuddin, and S. Datta, Nat. Nanotechnol. **5**, 266 (2010).
[7] N. Locatelli, V. Cros, and J. Grollier, Nat. Mater. **13**, 11 (2014).
[8] S. Lequeux, J. Sampaio, V. Cros, K. Yakushiji, A. Fukushima, R. Matsumoto, H. Kubota, S. Yuasa, and J. Grollier, Sci. Rep. **6**, 31510 (2016).
[9] T. Ono, H. Miyajima, K. Shigeto, K. Mibu, N. Hosoito, and T. Shinjo, Science **284**, 468 (1999).
[10] D. Atkinson, D. A. Allwood, G. Xiong, M. D. Cooke, C. C. Faulkner, and R. P. Cowburn, Nat. Mater. **2**, 85 (2003).
[11] Y. Nakatani, A. Thiaville, and J. Miltat, Nat. Mater. **2**, 521 (2003).
[12] G. S. D. Beach, C. Nistor, C. Knutson, M. Tsoi, and J. L. Erskine, Nat. Mater. **4**, 741 (2005).
[13] M. Kläui, C. A. F. Vaz, J. A. C. Bland, W. Wernsdorfer, G. Faini, E. Cambril, L. J. Heyderman, F. Nolting, and U. Rüdiger, Phys. Rev. Lett. **94**, 106601 (2005).
[14] M. Hayashi, L. Thomas, C. Rettner, R. Moriya, Y. B. Bazaliy, and S. S. P. Parkin, Phys. Rev. Lett. **98**, 037204 (2007).
[15] D. Ravelosona, S. Mangin, J. A. Katine, E. E. Fullerton, and B. D. Terris, Appl. Phys. Lett. **90**, 072508 (2007).
[16] A. V. Khvalkovskiy, V. Cros, D. Apalkov, V. Nikitin, M. Krounbi, K. A. Zvezdin, A. Anane, J. Grollier, and A. Fert, Phys. Rev. B **87**, 020402 (2013).
[17] S.-H. Yang, K.-S. Ryu, and S. Parkin, Nat. Nanotechnol. **10**, 221 (2015).
[18] P. J. Metaxas, J. Sampaio, A. Chanthbouala, R. Matsumoto, A. Anane, A. Fert, K. A. Zvezdin, K. Yakushiji, H. Kubota, A. Fukushima, S. Yuasa, K. Nishimura, Y. Nagamine, H. Maehara, K. Tsunekawa, V. Cros, and J. Grollier, Sci. Rep. **3**, 1829 (2013).
[19] J. Dean, M. T. Bryan, T. Schrefl, and D. A. Allwood, J. Appl. Phys. **109**, 023915 (2011).
[20] M. T. Bryan, J. Dean, and D. A. Allwood, Phys. Rev. B **85**, 144411 (2012).
[21] H. Sohn, M. E. Nowakowski, C. Y. Liang, J. L. Hockel, K. Wetzlar, S. Keller, B. M. McLellan, M. A. Marcus, A. Doran,

A. Young, M. Kläui, G. P. Carman, J. Bokor, and R. N. Candler, ACS Nano **9**, 4814 (2015).

[22] J.-M. Hu, T. Yang, K. Momeni, X. Cheng, L. Chen, S. Lei, S. Zhang, S. Trolier-McKinstry, V. Gopalan, G. P. Carman, C.-W. Nan, and L.-Q. Chen, Nano Lett. **16**, 2341 (2016).

[23] E. Mikheev, I. Stolichnov, E. De Ranieri, J. Wunderlich, H. J. Trodahl, A. W. Rushforth, S. W. E. Riester, R. P. Campion, K. W. Edmonds, B. L. Gallagher, and N. Setter, Phys. Rev. B **86**, 235130 (2012).

[24] J. H. Franken, Y. Yin, A. J. Schellekens, A. van den Brink, H. J. M. Swagten, and B. Koopmans, Appl. Phys. Lett. **103**, 102411 (2013).

[25] N. Lei, T. Devolder, G. Agnus, P. Aubert, L. Daniel, J.-V. Kim, W. Zhao, T. Trypiniotis, R. P. Cowburn, C. Chappert, D. Ravelosona, and P. Lecoeur, Nat. Commun. **4**, 1378 (2013).

[26] E. De Ranieri, P. E. Roy, D. Fang, E. K. Vehsthedt, A. C. Irvine, D. Heiss, A. Casiraghi, R. P. Campion, B. L. Gallagher, T. Jungwirth, and J. Wunderlich, Nat. Mater. **12**, 808 (2013).

[27] B. Van de Wiele, L. Laurson, K. J. A. Franke, and S. van Dijken, Appl. Phys. Lett. **104**, 012401 (2014).

[28] K. J. A. Franke, B. Van de Wiele, Y. Shirahata, S. J. Hämäläinen, T. Taniyama, and S. van Dijken, Phys. Rev. X **5**, 011010 (2015).

[29] N. A. Pertsev, Appl. Phys. Lett. **102**, 112407 (2013).

[30] N. Tiercelin, Y. Dusch, A. Klimov, S. Giordano, V. Preobrazhensky, and P. Pernod, Appl. Phys. Lett. **99**, 192507 (2011).

[31] S. Giordano, Y. Dusch, N. Tiercelin, P. Pernod, and V. Preobrazhensky, Phys. Rev. B **85**, 155321 (2012).

[32] Y. Dusch, N. Tiercelin, A. Klimov, S. Giordano, V. Preobrazhensky, and P. Pernod, J. Appl. Phys. **113**, 17C719 (2013).

[33] S. Giordano, Y. Dusch, N. Tiercelin, P. Pernod, and V. Preobrazhensky, Eur. Phys. J. B **86**, 249 (2013).

[34] S. Giordano, Y. Dusch, N. Tiercelin, P. Pernod, and V. Preobrazhensky, J. Phys. D: Appl. Phys. **46**, 325002 (2013).

[35] A. K. Biswas, S. Bandyopadhyay, and J. Atulasimha, Appl. Phys. Lett. **104**, 232403 (2014).

[36] H. Ahmad, J. Atulasimha, and S. Bandyopadhyay, Sci. Rep. **5**, 18264 (2015).

[37] C.-Y. Liang, A. Sepulveda, S. Keller, and G. P. Carman, J. Appl. Phys. **119**, 113903 (2016).

[38] T. Mathurin, S. Giordano, Y. Dusch, N. Tiercelin, P. Pernod, and V. Preobrazhensky, Appl. Phys. Lett. **108**, 082401 (2016).

[39] T. Mathurin, S. Giordano, Y. Dusch, N. Tiercelin, P. Pernod, and V. Preobrazhensky, Eur. Phys. J. B **89**, 169 (2016).

[40] N. L. Schryer and L. R. Walker, J. Appl. Phys. **45**, 5406 (1974).

[41] See Supplemental Material at http://link.aps.org/supplemental/10.1103/PhysRevB.95.140405 for additional details on the system description, the comparison with micromagnetic simulations, and a discussion on the domain-wall shape.

[42] F. Cayssol, D. Ravelosona, C. Chappert, J. Ferré, and J. P. Jamet, Phys. Rev. Lett. **92**, 107202 (2004).

[43] L. Landau and E. Lifshits, Phys. Zeitsch. der Sow. **8**, 153 (1935).

[44] T. L. Gilbert, Phys. Rev. **100**, 1243 (1955); IEEE Trans. Mag. **40**, 3443 (2004).

[45] F. Wang, L. Luo, D. Zhou, X. Zhao, and H. Luo, Appl. Phys. Lett. **90**, 212903 (2007).

[46] N. A. Pertsev, Phys. Rev. B **78**, 212102 (2008).

[47] Y. Dusch, N. Tiercelin, A. Klimov, V. Rudenko, Y. Ignatov, S. Hage-Ali, P. Pernod, and V. Preobrazhensky, J. Appl. Phys. **109**, 07A720 (2011).